

## Measurement-induced quantum walks on an IBM quantum computer

Sabine Tornow, Klaus Ziegler


### Angaben zur Veröffentlichung / Publication details:

Tornow, Sabine, and Klaus Ziegler. 2023. "Measurement-induced quantum walks on an IBM quantum computer." *Physical Review Research* 5 (3): 033089.  
<https://doi.org/10.1103/physrevresearch.5.033089>.

# Measurement-induced quantum walks on an IBM quantum computer

Sabine Tornow 

*Research Institute CODE, Universität der Bundeswehr München, Carl-Wery-Straße 22, 81739 Munich, Germany*

Klaus Ziegler 

*Institut für Physik, Universität Augsburg, 86135 Augsburg, Germany*



(Received 25 October 2022; accepted 7 June 2023; published 8 August 2023)

We study a quantum walk of a single particle that is subject to stroboscopic projective measurements on a graph with two sites. This two-level system is the minimal model of a measurement-induced quantum walk. The mean first detected transition and return time are computed on an IBM quantum computer as a function of the hopping matrix element between the sites and the on-site potential. The experimentally monitored quantum walk reveals the theoretically predicted behavior, such as the quantization of the first detected return time and the strong increase of the mean first detected transition time near degenerate points, with high accuracy.

DOI: [10.1103/PhysRevResearch.5.033089](https://doi.org/10.1103/PhysRevResearch.5.033089)

## I. INTRODUCTION

Quantum walks are a central concept for quantum information processing [1,2] as they are indispensable for quantum algorithm development and for modeling of physical processes. Furthermore, they provide a universal model of quantum computation [3] and can be considered as a quantum version of the classical random walk [4]. Measurement-induced quantum walks [5] present a special class of quantum walks for which the unitary time evolution is supplemented by a (projective) measurement, resulting in a nonunitary evolution. To study this effect on a quantum computer, we consider a closed quantum system that is subject to repeated identical projective (stroboscopic) measurements and that evolves unitarily between two successive measurements. The combined evolution of the system is nonunitary and can be understood as a monitored evolution (ME) which has some surprising properties. Assuming stroboscopic measurements, where a projection is applied repeatedly after a fixed time interval  $\tau$ , we count the number of measurements to observe a certain quantum state for the first time. This number depends on the size of the underlying Hilbert space, the time interval  $\tau$ , the detected state, and the initial state, in which the quantum system was prepared. We must distinguish two different cases: the first detected return (FDR), where the initial state and the measured state are identical, and the first detected transition (FDT), where the initial state and the measured state are different. The FDR has been intensively studied and revealed some remarkable properties [6–15]: The mean FDR time  $\tau\langle n \rangle$  is quantized, where  $\langle n \rangle$  is an integer and equal to or less than the number of contributing energy levels [6,7]. Degenerate energy

levels count only once. This implies that  $\langle n \rangle$  jumps if we tune the system through a degeneracy. The quantization is related to the integer winding number of the Laplace transform of the return amplitude [6,14] and exists also for random time steps  $\{\tau_j\}$  when we average with respect to their distribution [16]. In the latter case, the mean FDR time is formally a Berry phase integral due to the time-averaged measurements. The mean FDT time, on the other hand, is not quantized but has characteristic divergences near degenerate energy levels [17–19].

Neither the quantization of the mean FDR time nor the divergences of the mean FDT time have been observed experimentally. However, due to the fast improvement of current quantum computers, including the possibility to implement midcircuit measurements, which are, e.g., crucial for the realization of quantum error correction protocols [20], these computers provide an excellent platform for testing the theory of the ME with stroboscopic measurements directly. For this purpose, a tight-binding model on a finite graph is realized on an IBM quantum computer to study the mean FDR time and its fluctuations as well as the mean FDT time experimentally. In this work we focus on the simplest case of a two-site graph with one particle which is already sufficient to observe the characteristic features of the ME, as described above. Such a system is implemented on the IBM quantum computer with one and with two qubits. For a small number of midcircuit measurements, the error-mitigated results are found to be in very good agreement with the theoretically predicted exact results. In this context we calculate the error due to a finite number  $N$  of measurements (typically  $N \approx 40$ ) in comparison to the infinite number of measurements assumed in the theory. It turns out that this error is exponentially small, as presented in the [Appendix](#).

The paper is organized as follows. Section II is the theoretical part that describes the model and the ME. A detailed explanation of how the model is implemented on the quantum computer and a discussion of an appropriate error-mitigation

*Published by the American Physical Society under the terms of the Creative Commons Attribution 4.0 International license. Further distribution of this work must maintain attribution to the author(s) and the published article's title, journal citation, and DOI.*

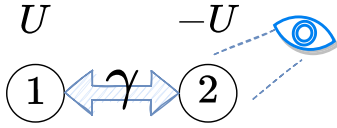


FIG. 1. Scheme of the tight-binding model with two sites. The quantum particle is prepared on the initial site 2 and periodically measured (indicated with the eye). Here  $U$  and  $\gamma$  denote the strength of the potential and the hopping matrix element, respectively.

scheme are provided in Sec. III. In Sec. IV we present the experiments for the FDR/FDT times as well as their variance. We summarize our results in Sec. V and propose some ideas for future studies.

## II. MODEL

The tight-binding model for a quantum particle on a finite chain of length  $l$  is described by the particle-number-conserving Hamiltonian

$$H = \sum_{j=1}^l [-\gamma_{j,j+1}(|j\rangle\langle j+1| + |j+1\rangle\langle j|) + U_j |j\rangle\langle j|]$$

with proper boundary conditions. This tight-binding Hamiltonian is encoded by the qubit Hamiltonian

$$H_l = \sum_{j=1}^l [U_j \sigma_{z,j} - \gamma_{j,j+1}(\sigma_{x,j} \sigma_{x,j+1} + \sigma_{y,j} \sigma_{y,j+1})], \quad (1)$$

where  $\sigma_x$ ,  $\sigma_y$ , and  $\sigma_z$  are Pauli matrices. The states  $|0 \dots 01\rangle$ ,  $|0 \dots 10\rangle$ ,  $\dots$ ,  $|10 \dots 0\rangle$  encode the position of the particle at site  $1, 2, \dots, l$  along the chain. The first term of the Hamiltonian represents the on-site energy  $U_i$  on each site  $i$  and the second term represents the kinetic energy, parametrized by the hopping matrix element  $\gamma$  between neighboring sites.

Now we consider a particle moving on two sites and prepared initially on site 1 or 2 at time  $t = 0$ , which is measured stroboscopically on site 2 after the time  $\tau, 2\tau, \dots$  (see Fig. 1). The two-site Hamiltonian  $H_2$  acts on the computational basis states  $|10\rangle$  and  $|01\rangle$  as sites 1 and 2 in our model, respectively. The states  $|00\rangle$  and  $|11\rangle$  should not be populated. Since only two states are occupied, we can simplify the two-qubit model described by the Hamiltonian in Eq. (1) to a single-qubit problem with the two basis states  $|0\rangle = |01\rangle$  and  $|1\rangle = |10\rangle$ . In this basis the Hamiltonian matrix reads

$$(\langle j| H_2 |j'\rangle) = -\gamma \sigma_x + U \sigma_z = \begin{pmatrix} U & -\gamma \\ -\gamma & -U \end{pmatrix}, \quad (2)$$

whose eigenenergies are  $E_{1,2} = \pm \sqrt{U^2 + \gamma^2}$ .

The ME with  $n$  stroboscopic measurements is defined by the evolution operator [14,19]

$$M_n = e^{-iH_2\tau} (P e^{-iH_2\tau})^{n-1}, \quad P = \mathbf{1} - |j\rangle\langle j| = |j'\rangle\langle j'|, \quad (3)$$

with  $j, j' \in \{0, 1\}$  and  $j' \neq j$ , which can also be written for  $n \geq 2$  as

$$M_n = e^{-iH_2\tau} |j'\rangle\langle j'| (e^{-iH_2\tau})^{n-2} |j'\rangle\langle j'| e^{-iH_2\tau}. \quad (4)$$

Then the FDR probability  $|\phi_{r,n}|^2 = |\langle j| M_n |j\rangle|^2$  for  $|j\rangle \rightarrow |j\rangle$  reads

$$\begin{cases} |\langle j| e^{-iH_2\tau} |j\rangle|^2 & \text{for } n = 1, \\ |\langle j'| e^{-iH_2\tau} |j'\rangle|^{2n-4} |\langle j| e^{-iH_2\tau} |j'\rangle \langle j'| e^{-iH_2\tau} |j\rangle|^2 & \text{for } n \geq 2 \end{cases} \quad (5)$$

and the FDT probability  $|\phi_{t,n}|^2 = |\langle j'| M_n |j\rangle|^2$  for  $|j\rangle \rightarrow |j'\rangle$  reads

$$|\langle j'| e^{-iH_2\tau} |j'\rangle|^{2(n-1)} |\langle j'| e^{-iH_2\tau} |j\rangle|^2.$$

For the Hamiltonian  $H_2$  with  $U = 0$  we get  $|\langle j'| e^{-iH_2\tau} |j'\rangle|^2 = \cos^2(\gamma\tau)$  and  $|\langle j'| e^{-iH_2\tau} |j\rangle|^2 = \sin^2(\gamma\tau)$ . Similar but slightly more complex results are obtained for the parameter  $c = \cos(\sqrt{U^2 + \gamma^2}\tau)$  in the general case with  $U \neq 0$ . Then, for  $U = 0$  the distribution function  $|\phi_{r,n}|^2$  depends on  $c = \cos(\gamma\tau)$  and reads

$$|\phi_{r,n}|^2 = \begin{cases} c^2, & n = 1 \\ (1 - c^2)^2 c^{2(n-2)}, & n > 1 \end{cases} \quad (6)$$

for the FDR probability and for the FDT probability

$$|\phi_{t,n}|^2 = (1 - c^2) c^{2(n-1)}. \quad (7)$$

Thus, the sum of the FDR probabilities for all  $n \geq 1$  gives 1 and the mean FDR time is  $\tau \langle n \rangle$ . Subsequently, we will call  $\langle n \rangle$  the mean FDR time, assuming that it is implicitly multiplied by the time step  $\tau$ .

Here  $c^2 = 1$  plays a special role because then the transition  $|j\rangle \rightarrow |j'\rangle$  is completely suppressed:

$$\langle n \rangle = \sum_{n \geq 1} n |\phi_{r,n}|^2 = \begin{cases} 2, & c^2 < 1 \\ 1, & c^2 = 1. \end{cases} \quad (8)$$

The corresponding results of the FDT probabilities are

$$\sum_{n \geq 1} |\phi_{t,n}|^2 = \begin{cases} 0, & c^2 = 1 \\ 1, & c^2 < 1, \end{cases} \quad (9)$$

$$\langle n \rangle = \sum_{n \geq 1} n |\phi_{t,n}|^2 = \begin{cases} 0, & c^2 = 1 \\ 1/(1 - c^2), & c^2 < 1. \end{cases} \quad (10)$$

These FDR/FDT results are obtained for an infinite number of measurements. Since an experiment allows only a finite number of measurements, the corresponding mean FDR/FDT results for  $N$  measurements must be calculated separately. For instance, the mean FDR time reads (cf. the Appendix)

$$\langle n \rangle = \sum_{n=1}^N n |\phi_{r,n}|^2 = 2 + c^{2(N-1)} [N(c^2 - 1) - 1], \quad (11)$$

which gives  $\langle n \rangle \sim 2$  for  $c^2 < 1$ ,  $N \sim \infty$ , and  $\langle n \rangle = 1$  for  $c^2 = 1$ . The second moment reads

$$\langle n^2 \rangle = \frac{2 - c^{2(N-1)} [(N^2 - N)c^4 + 2(1 - N^2)c^2 + N^2 + N]}{1 - c^2}, \quad (12)$$

and for the mean FDT time we obtain

$$\langle n \rangle = \sum_{n=1}^N n |\phi_{t,n}|^2 = \frac{1 + c^{2N} [N(c^2 - 1) - 1]}{1 - c^2}. \quad (13)$$

An important difference is that  $\langle n \rangle$  in Eq. (10) diverges due to the infinite number of measurements for  $c^2 \sim 1$ , whereas it vanishes as  $1 - c^2$  for a finite number of measurements  $N$  in Eq. (13). Otherwise, the deviation due to a finite number of measurements is exponentially small.

### III. IMPLEMENTATION ON A QUANTUM COMPUTER

#### A. Single-qubit implementation

General operators, such as the unitary evolution operator  $\exp(-iH\tau)$ , must be constructed on a quantum computer as a product of elementary gate operators. For  $U = 0$  the time evolution is equal to single-qubit rotation about the  $X$  axis

$$e^{-i\gamma\sigma_x t} = \begin{pmatrix} \cos(\gamma t) & -i \sin(\gamma t) \\ -i \sin(\gamma t) & \cos(\gamma t) \end{pmatrix} \quad (14)$$

$$= R_x(2\gamma t) \quad (15)$$

and is implemented with an  $R_x$  gate.

In the case of  $U \neq 0$ , the parts of the Hamiltonian  $H_2$  are not commuting, so each part cannot be simulated separately. However, if the Hamiltonian  $H$  consists of a sum of simple qubit operators we can employ time slicing or Trotterization [21]. In terms of  $\exp(-iH_2\tau)$  this means that we divide the time  $\tau$  into  $k$  time slices  $\Delta t$  with  $\Delta t = \tau/k$ , which provides the approximation

$$e^{-iH_2\tau} \approx (e^{i\gamma\sigma_x \Delta t} e^{-iU\sigma_z \Delta t})^k. \quad (16)$$

In the limit  $k \rightarrow \infty$  the approximation becomes exact. Therefore, for a good approximation the Trotter number  $k$  must be large. In our case we obtained reliable results for  $k = 30$ . In the single-qubit case of  $H_2$  we have

$$e^{-i\gamma\sigma_x \Delta t} = \begin{pmatrix} \cos(\gamma \Delta t) & -i \sin(\gamma \Delta t) \\ -i \sin(\gamma \Delta t) & \cos(\gamma \Delta t) \end{pmatrix} \quad (17)$$

$$= R_x(2\gamma \Delta t) \quad (18)$$

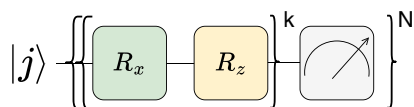
and

$$e^{-iU\sigma_z \Delta t} = \begin{pmatrix} e^{-iU \Delta t} & 0 \\ 0 & e^{iU \Delta t} \end{pmatrix} = R_z(2U \Delta t) \quad (19)$$

such that the single-qubit unitary operator can be written as

$$e^{-iH_2\tau} \approx \{R_z(2U \Delta t)R_x(2\gamma \Delta t)\}^k. \quad (20)$$

The unitary evolution is followed by a projective measurement in the computational basis, defined by the projectors  $P_0 = |0\rangle\langle 0|$  and  $P_1 = |1\rangle\langle 1|$ . To implement the unitary operator in Eq. (20), followed by projective measurements, we run the quantum circuit (circuit 1) on the quantum device



where  $k$  denotes the number of Trotter steps and  $N$  the number of measurements. The gates  $R_z$  and  $R_x$  implement the rotations  $R_z(2U \Delta t)$  and  $R_x(2\gamma \Delta t)$  in Eq. (20), respectively, and the initial state  $|j\rangle$  is either  $|0\rangle$  or  $|1\rangle$ .

#### B. Two-qubit implementation

In analogy to the single-qubit case, we approximate the unitary time evolution for two qubits with the Hamiltonian

$$H_2^2 = -\gamma(\sigma_x \otimes \sigma_x + \sigma_y \otimes \sigma_y) + U\sigma_0 \otimes \sigma_z \quad (21)$$

as

$$e^{-iH_2^2 t} \approx (e^{i\gamma\sigma_x \otimes \sigma_x \Delta t} e^{i\gamma\sigma_y \otimes \sigma_y \Delta t} e^{-iU\sigma_0 \otimes \sigma_z \Delta t})^k. \quad (22)$$

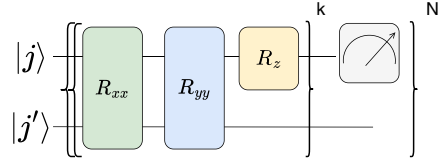
The single factors are written in the basis of  $|00\rangle, \dots, |11\rangle$  as

$$\begin{aligned} e^{i\gamma\sigma_x \otimes \sigma_x \Delta t} e^{i\gamma\sigma_y \otimes \sigma_y \Delta t} \\ = R_{xx}(2\gamma \Delta t) R_{yy}(2\gamma \Delta t) \\ = \begin{pmatrix} 1 & 0 & 0 & 0 \\ 0 & \cos(2\gamma \Delta t) & -i \sin(2\gamma \Delta t) & 0 \\ 0 & -i \sin(2\gamma \Delta t) & \cos(2\gamma \Delta t) & 0 \\ 0 & 0 & 0 & 1 \end{pmatrix} \end{aligned} \quad (23)$$

and

$$\begin{aligned} e^{i(U\sigma_0 \otimes \sigma_z \Delta t)} = \sigma_0 \otimes R_z(2U \Delta t) \\ = \begin{pmatrix} e^{-iU \Delta t} & 0 & 0 & 0 \\ 0 & e^{iU \Delta t} & 0 & 0 \\ 0 & 0 & e^{-iU \Delta t} & 0 \\ 0 & 0 & 0 & e^{iU \Delta t} \end{pmatrix}. \end{aligned} \quad (24)$$

The corresponding quantum circuit (circuit 2) can be visualized as



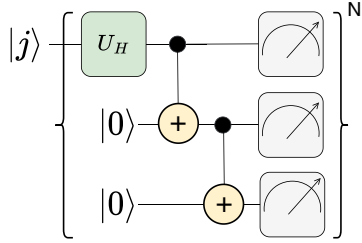
where the gates  $R_z$ ,  $R_{yy}$ , and  $R_{xx}$  implement the rotations  $R_z(2U \Delta t)$ ,  $R_{yy}(2\gamma \Delta t)$ , and  $R_{xx}(2\gamma \Delta t)$ , respectively. The initial states  $|j\rangle$  and  $|j'\rangle$  are either  $|0\rangle$  or  $|1\rangle$  and only the first qubit is projectively measured.

#### C. Error mitigation

In general, there are several sources of errors on current quantum computing devices, e.g., amplitude damping, phase damping, depolarization, state preparation, and measurement errors. In this work we focus on the mitigation of the latter as we implement quantum circuits with up to 40 midcircuit measurements and therefore anticipate that measurement errors have the most significant impact on our experimental results.

Many readout-error-mitigation schemes rely on classical postprocessing techniques that involve measuring a calibration matrix and applying this matrix to the raw experimental data, which would render readout-error mitigation inefficient and time consuming in our case. Furthermore, due to the relatively high number of measurements, a regular updating of the measurement calibration matrix would be necessary. Therefore, we use a readout-error-mitigation technique that is better suited for a high number of midcircuit measurements. This scheme employs the framework of quantum error correction and embeds the state after the application of a unitary

gate and before a measurement in a nonlocal state of three entangled qubits, analogous to the encoding in the three-qubit repetition code, as depicted in the following quantum circuit (circuit 3):



This three-qubit repetition code is able to mitigate bit-flip errors by performing a majority vote after each measurement sequence [22,23]. This technique in particular is successful if readout errors dominate the two-qubit gate errors, which is the case if the distribution function  $|\phi_n|^2$  has most of its weight at low number of measurement  $n$  and therefore the result depends only on the first few measurements.

For the two-qubit quantum circuits we are using an error-detection approach. Errors are detected by measuring both qubits and are present if the states  $|00\rangle$  and  $|11\rangle$  are measured. The data where errors are detected are disregarded.

#### IV. FIRST DETECTED RETURN AND TRANSITION EXPERIMENTS

We use IBM's open-source QISKIT library for quantum computing. QISKIT provides tools for different tasks such as creating Trotter expansions, quantum circuits with midcircuit measurements, performing simulations, and computations on real quantum devices [24]. Since only a finite number of midcircuit measurement is possible on the real hardware, we discuss the dependence of the result on the number of measurements  $N$  in the Appendix.

We perform the experiments by initializing a particle on site 2, letting it freely evolve for some time before we measure if the particle is on site 1 (site 2), and repeat this process  $n$  times until we detect the particle on site 1 (site 2) as visualized in Fig. 1. Based on the stroboscopic measurement protocol, the statistics of the FDR time shows that the mean  $\langle n \rangle$  is quantized and equal to 2 in the two-site tight-binding problem, except for the degenerate points, where the potential  $U$  is

$$U_d = \sqrt{\frac{\pi^2 k^2}{\tau^2} - \gamma^2} \quad (k = 1, 2, \dots). \quad (25)$$

In that case we have  $\cos^2(\sqrt{U_d^2 + \gamma^2}\tau) = 1$  and get  $|\phi_{r,1}|^2 = 1$ , according to Eq. (6), and  $\langle n \rangle = 1$ . Therefore, the particle is measured at the first measurement with certainty.

We start with the one-qubit experiments (qubit 12 on IBMQ Montreal) with 32 000 runs for  $U = 0$ ,  $\tau = 0.4$ , and varying  $\gamma$ . We initialize the qubit in state  $|1\rangle$  and perform alternately an  $x$  rotation and a measurement in the  $z$  basis  $N = 40$  times according to circuit 1. The result is postprocessed to obtain the FDT (FDR) probability  $|\phi_{t,n}|^2$  ( $|\phi_{r,n}|^2$ ) by evaluating the counts and  $n$  where the initial state and the

measured state are for the first time different (the same), i.e., when the measured state is for the first time  $|0\rangle$  ( $|1\rangle$ ). From these probabilities we can calculate the mean  $\langle n \rangle$ , as defined in Eqs. (8) and (10), as well as its second moments  $\langle n^2 \rangle$  for a finite number of measurements (cf. the Appendix). The mean FDR time  $\langle n \rangle$  at  $U = 0$  is computed on IBMQ Montreal with and without error mitigation, with results depicted in Fig. 2(a). It clearly shows the quantization  $\langle n \rangle = 2$  as well as the degenerate points at  $\gamma = \pi k / \tau$ , with  $\gamma = 0$ ,  $\gamma = \pi / \tau \approx 7.85$ , and  $\gamma = 2\pi / \tau \approx 15.7$  ( $\tau = 0.4$ ), where  $\langle n \rangle = 1$  as expected. At these points the variance  $\langle n^2 \rangle - \langle n \rangle^2$  shows the theoretically expected divergences in Fig. 2(b). The experimental values are in very good quantitative agreement with the exact results for  $N = 40$  measurements and are improved by the repetition-code error-mitigation scheme introduced in Sec. III C (see circuit 3).

In Fig. 2(c) the exact FDR probability is visualized as a function of the hopping matrix element  $\gamma$  and the number of measurements. This agrees very well with the experimental results of the corresponding FDR probability on IBMQ Montreal without error mitigation in Fig. 2(d).

According to the theory, the FDT time for the hopping to another site has different properties. Its mean FDT is not quantized and diverges already near the degeneracy  $U_d$ . The results for the same parameter as for the FDR are presented in Fig. 3. In Fig. 3(a) the mean FDR time is small and close to one and it grows near the degeneracy points at  $\gamma = \pi k / \tau$ , when the particle remains on the initial site. The exact results of the mean FDT time for  $N = 40$  measurements do not diverge at the degenerate points but are zero (cf. the Appendix), in contrast to their divergence for  $N \rightarrow \infty$ . The experiment shows a finite nonzero value. This is due to the fact that the qubit decays at a smaller  $n$ , visible by comparing Figs. 3(c) and 3(d): The experimental FDT probability  $|\phi_{t,n}|^2$  is nonzero and not exactly zero as in Eq. (7).

To investigate further the mean FDR and FDT times for varying  $\gamma$ , we consider the two-qubit experiments on IBMQ Montreal (qubits 12 and 13) with 32 000 runs for  $U = 0$ ,  $\tau = 0.4$ , and varying  $\gamma$ . We initialize the qubit in the state  $|01\rangle$  and perform alternately a two-qubit  $xx$  rotation and  $yy$  rotation and perform a measurement in the  $z$  basis of both qubits (for the error mitigation)  $N = 40$  times. The result is postprocessed to obtain the FDT (FDR) probability  $|\phi_{t,n}|^2$  ( $|\phi_{r,n}|^2$ ) by evaluating the counts and  $n$ , where the initial state and the measured state are different (FDT) or the same (FDR) for the first time. Besides the relevant states  $|10\rangle$  and  $|01\rangle$  for the ME, the system can also occupy  $|00\rangle$  or  $|11\rangle$ . Those contributions are used in our error-detection strategy.

We present results in Fig. 4, with and without error mitigating. Similar to the one-qubit case, the mean FDR quantization ( $\langle n \rangle = 2$ ) is clearly visible in the error-mitigated data of Fig. 4(a), while the raw experimental data in Figs. 4(a) and 4(c) is more noisy and the mean FDR time is slightly larger than 2. Nonetheless, the effect of degenerate points is clearly visible also in the mean FDT time of Fig. 4(b), where  $\langle n \rangle$  decreases at the degenerate points, as expected from the exact curve at  $N = 40$ . In Fig. 4(d) the experimental FDT probability  $|\phi_{t,n}|^2$  is close to zero at the degenerate points, in contrast to the one-qubit case of Fig. 3(a).



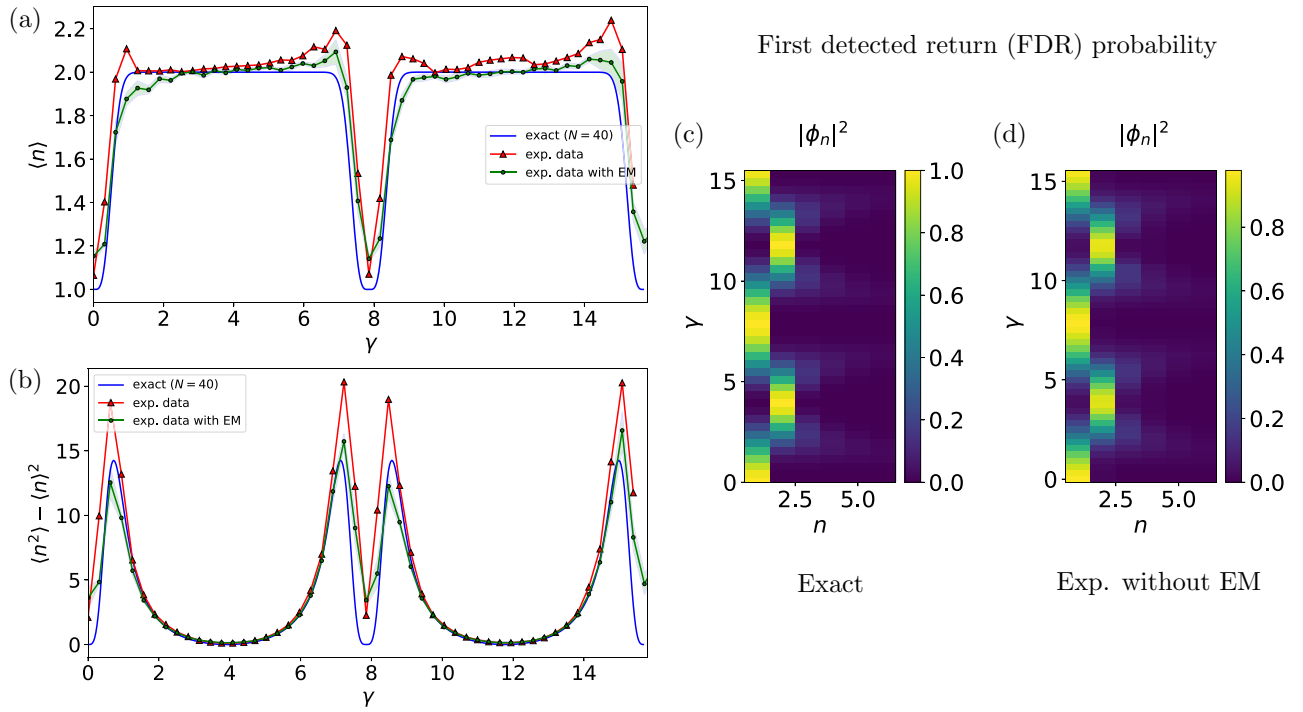


FIG. 2. Single-qubit experiment ( $U = 0$ ): (a) mean FDR time  $\langle n \rangle$  and (b) variance of  $n$  of the two-site system for the return  $|1\rangle \rightarrow |1\rangle$  for  $\tau = 0.4$  and  $N = 40$  as a function of the hopping matrix  $\gamma$  is calculated theoretically (blue solid line) and computed on IBMQ Montreal with (green circles) and without error mitigation (EM) (red triangles). The green shaded area marks the standard deviation of the error-mitigated result. The FDR probability of the ME  $|\phi_{r,n}|^2$  as a function of  $\gamma$  and number of measurements  $n$  is presented for the theory in (a) and for the experiment on IBMQ Montreal without error mitigation in (b). Also shown is the FDR probability of the monitored evolution  $|\phi_{r,n}|^2$  as a function of  $\gamma$  and (c) the number of measurements simulated and (d) experimental data from IBMQ Montreal without error mitigation.

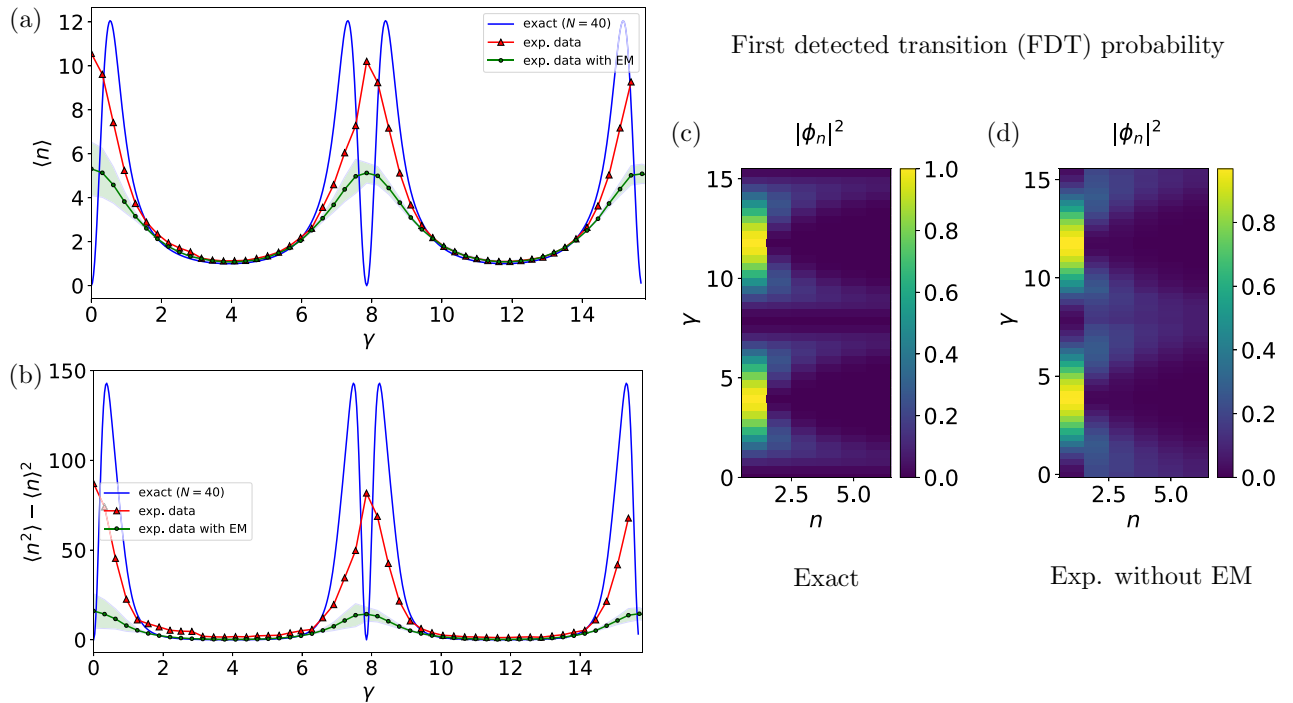


FIG. 3. Single-qubit experiment ( $U = 0$ ): (a) mean FDT time  $\langle n \rangle$  and (b) variance of  $n$  for the same system and the same model parameters as in Fig. 2. The blue solid curve is the theoretical result, while the computation on IBMQ Montreal is presented with error mitigation (green circles) and without (red triangles). The green shaded area marks the standard deviation of the error-mitigated result. Also shown is the FDT probability of the ME as a function of  $\gamma$  and (c) the number of measurements from theory and (d) the experiment on IBMQ Montreal without error mitigation.

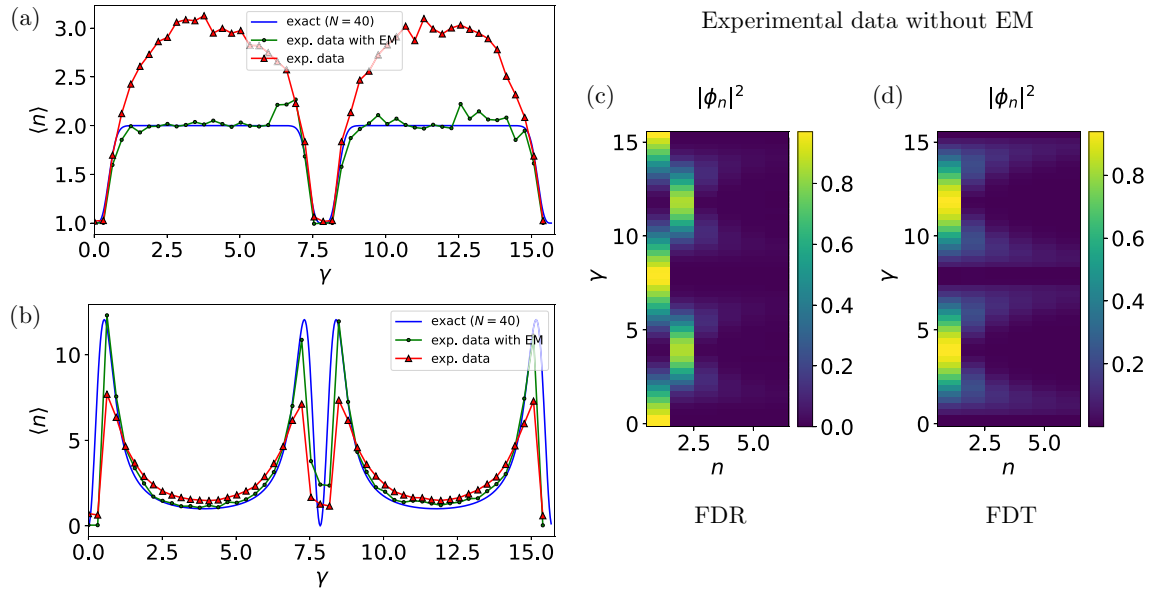


FIG. 4. Two-qubit experiment ( $U = 0$ ): (a) mean FDR time  $\langle n \rangle$  of the two-site system for the return  $|01\rangle \rightarrow |01\rangle$  and (b) mean FDT time  $\langle n \rangle$  of the two-site system for the transition  $|01\rangle \rightarrow |10\rangle$  for  $\tau = 0.4$  and  $N = 40$  as a function of the exact hopping matrix element  $\gamma$  (blue solid line) and computed on IBMQ Montreal with (green circles) and without error mitigation (red triangles). The standard deviation is approximately 0.5 and is not shown for better visibility. (c) FDR probability of the monitored evolution  $|\phi_{r,n}|^2$  as a function of  $\gamma$  and number of measurements on IBMQ Montreal without error mitigation. (d) FDT probability of the monitored evolution  $|\phi_{t,n}|^2$  as a function of  $\gamma$  and number of measurements on IBMQ Montreal without error mitigation.

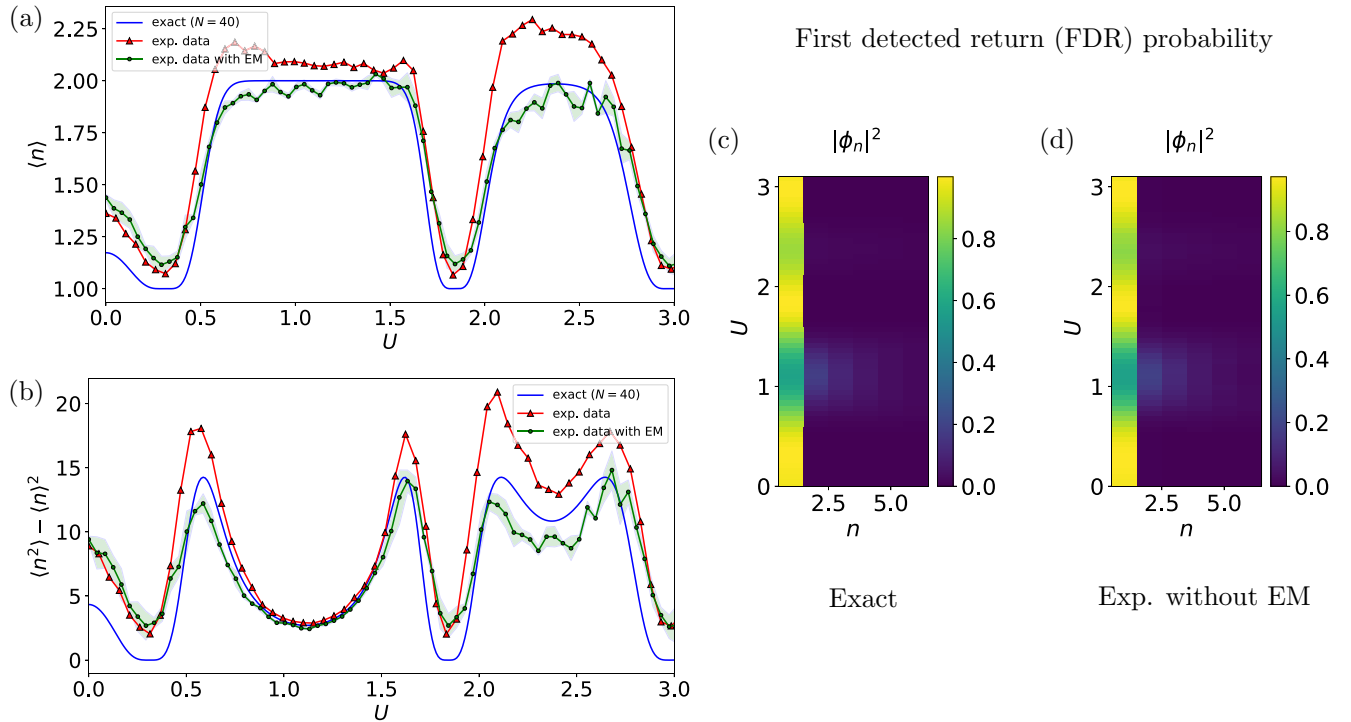


FIG. 5. Single-qubit experiment ( $U > 0$ ): (a) mean FDR time  $\langle n \rangle$  and (b) variance of  $n$  of the two-site system for the return  $|1\rangle \rightarrow |1\rangle$  for  $\gamma = -1$ ,  $\tau = 3$  ( $\Delta t = 0.1$  and  $k = 30$ ), and  $N = 40$  as a function of the on-site energy  $U$  exact (blue solid line) and computed on IBMQ Montreal with (green circles) and without error mitigation (red triangles). The green shaded area shows the standard deviation of the error-mitigated result. (c) FDR probability of the monitored evolution  $|\phi_{r,n}|^2$  as a function of  $U$  and number of measurements (exact). (d) FDR probability of the monitored evolution  $|\phi_{r,n}|^2$  as a function of  $U$  and number of measurements computed on IBMQ Montreal without error mitigation.

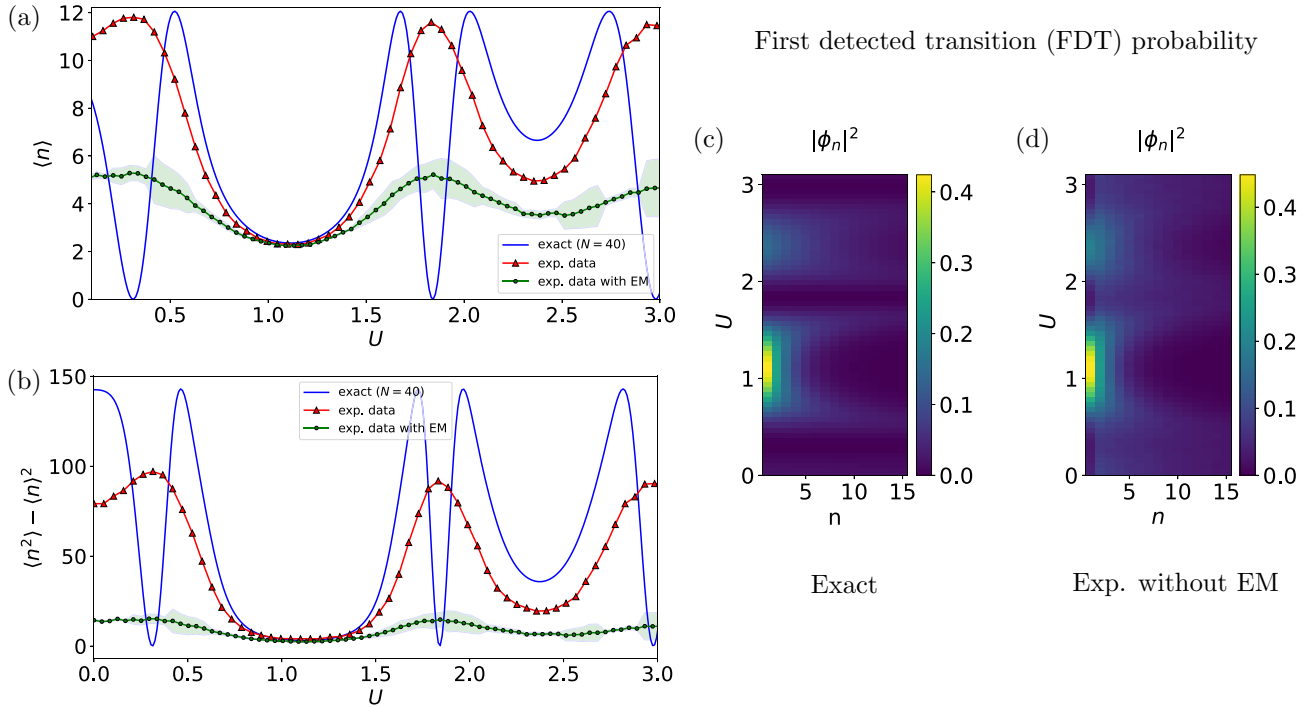


FIG. 6. Single-qubit experiment ( $U > 0$ ): (a) mean FDT time  $\langle n \rangle$  and (b) variance of  $n$  for the same system and the same model parameters as in Fig. 5. The blue solid curve is the theoretical result, while the computation on IBMQ Montreal is presented with error mitigation (green circles) and without (red triangles). The green shaded area marks the standard deviation of the error-mitigated result. Also shown is the FDT probability of the ME (c) as a function of  $U$  and the number of measurements from theory and (d) for the experiment on IBMQ Montreal without error mitigation.

Next we compute the two-site system with an on-site potential  $U$  on IBMQ Montreal. The mean FDR time  $\langle n \rangle$  is displayed as a function of  $U$  in Fig. 5. We perform the one-qubit experiments (qubit 12 on IBMQ Montreal) with 32 000 runs for  $\gamma = -1$ ,  $\tau = 3$ , and varying  $U$ , after initializing the qubit in state  $|1\rangle$  and perform alternating  $x$  and  $z$  rotations and a measurement in the  $z$  basis for  $N = 40$  on circuit 1 with  $\Delta t = 0.1$  and  $k = 30$  Trotter steps. Again, the mean FDR time is  $\langle n \rangle = 2$ , except for  $\langle n \rangle = 1$  at the degenerate points  $U_d$  of Eq. (25). In the present case this is  $U_d \approx 0.31, 1.84$ , and  $2.98$ . The raw experimental data are in qualitative agreement and the error-mitigated data are in very good quantitative agreement with the exact results and the quantization of  $\langle n \rangle$ . The corresponding divergences of the variance  $\langle n^2 \rangle - \langle n \rangle^2$  are also experimentally confirmed for nonzero  $U$  in Figs. 5(a) and 5(b).

In Fig. 5(c) the exact FDR probability is shown as a function of the energy bias  $U$  and the number of measurements, and in Fig. 5(d) the corresponding measured FDR probability on IBMQ Montreal is presented without error mitigation. Both results are almost identical, like in the  $U = 0$  case for varying  $\gamma$ .

The mean FDT time in Fig. 6(a) shows the complementary behavior. In the case where the FDT probability is large at small  $n$  close to  $U = 1$ , the raw experimental findings are in very good qualitative agreement with the exact values. For larger  $U$  the main contribution originates from larger  $n$  [see Figs. 6(c) and 6(d)]; therefore, the measurement errors accumulate, leading only to a qualitative agreement of the

mean FDT time in Fig. 6(a) and its variance in Fig. 6(b). Here, eventually other error-mitigation methods should be introduced since the applied scheme is not able to mitigate the errors for deeper quantum circuits (due to the error rate induced by the two-qubit gates in circuit 3), which are needed to calculate the mean  $\langle n \rangle$  in the FDT case for varying  $U$ .

We have demonstrated experimentally with a high accuracy that for the FDR problem of a particle in a two-site system, the mean return time  $\langle n \rangle$  is quantized and equal to the dimension of the underlying Hilbert space with nondegenerate eigenvalues (in our case  $\langle n \rangle = 2$ ). Moreover, at the degenerate points we found  $\langle n \rangle = 1$ . In our two-site (two-level) problems, this reflects the situation, in which the particle stays at the initial site. Because the experiment involves a large number of midcircuit measurements, the readout-error mitigation is essential. We have successfully used an error-mitigation scheme that is based on the repetition code with majority vote and error detection when the depth of the quantum circuits is relatively short.

## V. CONCLUSION

We experimentally investigated a monitored evolution of a tight-binding Hamiltonian on a quantum device and computed the mean FDR and mean FDT times for a one-qubit and a two-qubit system, where repeated measurements interrupt the unitary evolution by a projection after a time step  $\tau$ . To this end, we exploited the capabilities of midcircuit measurements on IBM quantum devices. The predictions of



the general theory for a finite but large number of measurements are accurately confirmed by the quantum computation. The FDR probability distribution of the monitored evolution is in good quantitative agreement with the exact result. We experimentally verified the remarkable property of the FDR problem in a two-site system: The mean  $\langle n \rangle$  is quantized and equal to the size of the system (in our case 2) for all  $U$  and  $\gamma$ . The mean  $\langle n \rangle$  is reduced to 1 at the degenerate points, where the size of the system, i.e., the number of non-degenerate eigenvalues of  $\exp(-iH_2\tau)$ , is reduced to 1. In this case the quantum gates effectively act as an identity matrix, multiplied by a phase factor. The behavior is different for the FDT problem, since  $\langle n \rangle$  diverges near the degenerate points. While the experimental data are very accurate for the FDR mean times, confirming the quantization, the jumps at the degenerate points, and the strong fluctuations, the mean FDT times for a nonzero energy bias (finite  $U$ ) are less accurate. In particular, the behavior near the degenerate points requires further experimental improvement on the hardware as well as on error-mitigation scheme, since those results depend on the measurement of a deeper circuit. The latter might accumulate readout errors and two-qubit gate errors. The experimental data for a larger number of measurements will benefit from devices which are capable of performing and processing a larger number of midcircuit measurements.

Our results reflect the large potential of the capabilities provided by the IBM quantum computers in terms of midcircuit measurements. Our ME, in connection with the topologically protected quantization of the mean FDR time, establishes a very flexible and scalable method for testing the performance of a quantum computer. The simple example of a single particle on two sites already indicates the direction in which an improvement in terms of long-time behavior and more complex systems is necessary. Future work should consider (i) larger systems with more particles and (ii) the application of measurement-induced quantum walks to quantum control and quantum algorithms, e.g., for quantum search or constrained quantum optimization [25,26].

### ACKNOWLEDGMENTS

The authors thank Eli Barkai, Quancheng Liu, and Ruoyo Yin for insightful discussions. We acknowledge the use of IBM Quantum services for this work. The views expressed are those of the authors and do not reflect the official policy or position of IBM or the IBM Quantum team. In this paper we used IBMQ Montreal, which is an IBM Quantum Falcon Processor. We acknowledge financial support by the University of the Bundeswehr Munich.

### APPENDIX

From the distributions of the FDR and FDT probabilities (cf. the main text) we can calculate the sum of the probabilities and the moments of  $n$  for a finite number of measurements  $N$ . For instance, the sum of the FDR probabilities reads

$$\sum_{n=1}^N |\phi_{r,n}|^2 = 1 - (1 - c^2)c^{2(N-1)} \quad (\text{A1})$$

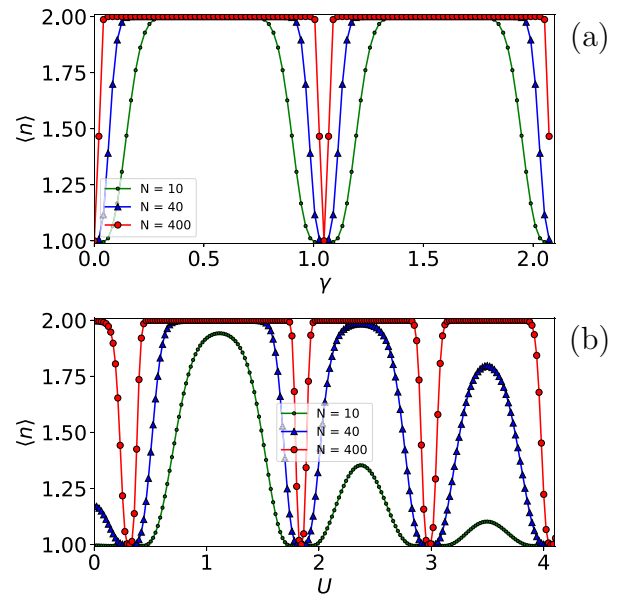


FIG. 7. Mean FDR time  $\langle n \rangle$  of the two-site system for the return  $|1\rangle \rightarrow |1\rangle$  as a function of (a)  $\gamma$  ( $\tau = 0.4$  and  $U = 0$ ) and (b)  $U$  ( $\tau = 3$  and  $\gamma = 1$ ) for different numbers of measurements  $N$ .

and the sum of the FDT probabilities

$$\sum_{n=1}^N |\phi_{t,n}|^2 = 1 - c^{2(N-1)}. \quad (\text{A2})$$

While the FDR sum is 1 for  $c^2 \leq 1$ , the FDT sum is 1 for  $c^2 < 1$  but vanishes for  $c^2 = 1$  in the limit  $N \rightarrow \infty$ . The latter reflects the fact that the two-level system always stays in the initial state if  $c^2 = 1$ , since the transition matrix element is

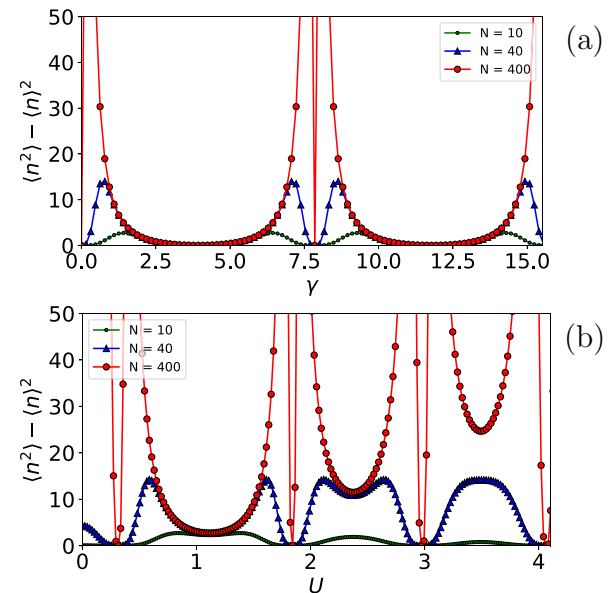


FIG. 8. Variance of the FDR time  $\langle n^2 \rangle - \langle n \rangle^2$  of the two-site system for the return  $|1\rangle \rightarrow |1\rangle$  as a function of (a)  $\gamma$  ( $\tau = 0.4$  and  $U = 0$ ) and (b)  $U$  ( $\tau = 3$  and  $\gamma = 1$ ) for different numbers of measurements  $N$ .

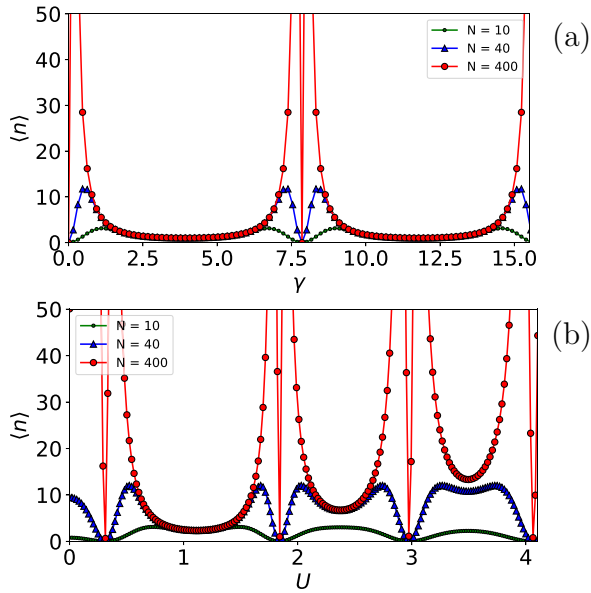


FIG. 9. Mean FDT time  $\langle n \rangle$  of the two-site system for the return  $|1\rangle \rightarrow |0\rangle$  as a function of (a)  $\gamma$  ( $\tau = 0.4$  and  $U = 0$ ) and (b)  $U$  ( $\tau = 3$  and  $\gamma = 1$ ) for different numbers of measurements  $N$ .

$1 - c^2$ . Moreover, for the mean FDR time  $\langle n \rangle$  we obtain

$$\langle n \rangle = \sum_{n=1}^N n |\phi_{r,n}|^2 = 2 + c^{2(N-1)} [N(c^2 - 1) - 1], \quad (\text{A3})$$

which gives  $\langle n \rangle \sim 2$  for  $c^2 < 1$ ,  $N \sim \infty$ , and  $\langle n \rangle = 1$  for  $c^2 = 1$ . The second moment reads

$$\langle n^2 \rangle = \frac{2 - c^{2(N-1)} [(N^2 - N)c^4 + 2(1 - N^2)c^2 + N^2 + N]}{1 - c^2}. \quad (\text{A4})$$

Finally, for the mean FDT time we obtain

$$\langle n \rangle = \sum_{n=1}^N n |\phi_{t,n}|^2 = \frac{1 + c^{2N} [N(c^2 - 1) - 1]}{1 - c^2}. \quad (\text{A5})$$

It should be noted that the last two expressions vanish for  $c^2 \rightarrow 1$  at any finite  $N$ , while they diverge when we take  $N \rightarrow \infty$  first and then  $c^2 \rightarrow 1$ . This means that the limits  $c^2 \rightarrow 1$  and  $N \rightarrow \infty$  do not commute. In Figs. 7–9 we plot the mean FDR time  $\langle n \rangle$  and variance of  $n$  as well as the mean FDT time for different numbers of measurements  $N$  as a function of  $U$  and  $\gamma$ .

- [1] Y. Aharonov, L. Davidovich, and N. Zagury, Quantum random walks, *Phys. Rev. A* **48**, 1687 (1993).
- [2] S. E. Venegas-Andraca, Quantum walks: A comprehensive review, *Quantum Inf. Process.* **11**, 1015 (2012).
- [3] A. M. Childs, Universal Computation by Quantum Walk, *Phys. Rev. Lett.* **102**, 180501 (2009).
- [4] A. M. Childs, E. Farhi, and S. Gutmann, An example of the difference between quantum and classical random walks, *Quantum Inf. Process.* **1**, 35 (2002).
- [5] A. Didi and E. Barkai, Measurement-induced quantum walks, *Phys. Rev. E* **105**, 054108 (2022).
- [6] F. A. Grünbaum, L. Velázquez, A. H. Werner, and R. F. Werner, Recurrence for discrete time unitary evolutions, *Commun. Math. Phys.* **320**, 543 (2013).
- [7] J. Bourgain, F. A. Grünbaum, L. Velázquez, and J. Wilkening, Quantum recurrence of a subspace and operator-valued Schur functions, *Commun. Math. Phys.* **329**, 1031 (2014).
- [8] S. Dhar, S. Dasgupta, A. Dhar, and D. Sen, Detection of a quantum particle on a lattice under repeated projective measurements, *Phys. Rev. A* **91**, 062115 (2015).
- [9] S. Dhar, S. Dasgupta, and A. Dhar, Quantum time of arrival distribution in a simple lattice model, *J. Phys. A: Math. Theor.* **48**, 115304 (2015).
- [10] P. Sinkovicz, T. Kiss, and J. K. Asbóth, Generalized Kac lemma for recurrence time in iterated open quantum systems, *Phys. Rev. A* **93**, 050101(R) (2016).
- [11] F. Thiel, E. Barkai, and D. A. Kessler, First Detected Arrival of a Quantum Walker on an Infinite Line, *Phys. Rev. Lett.* **120**, 040502 (2018).
- [12] D. Das and S. Gupta, Quantum random walk and tight-binding model subject to projective measurements at random times, *J. Stat. Mech.* (2022) 033212.
- [13] T. Nitsche, S. Barkhofen, R. Kruse, L. Sansoni, M. Štefaňák, A. Gábris, V. Potoček, T. Kiss, I. Jex, and C. Silberhorn, Probing measurement-induced effects in quantum walks via recurrence, *Sci. Adv.* **4**, eaar6444 (2018).
- [14] R. Yin, K. Ziegler, F. Thiel, and E. Barkai, Large fluctuations of the first detected quantum return time, *Phys. Rev. Res.* **1**, 033086 (2019).
- [15] S. Lahiri and A. Dhar, Return to the origin problem for a particle on a one-dimensional lattice with quasi-Zeno dynamics, *Phys. Rev. A* **99**, 012101 (2019).
- [16] K. Ziegler, E. Barkai, and D. Kessler, Randomly repeated measurements on quantum systems: Correlations and topological invariants of the quantum evolution, *J. Phys. A: Math. Theor.* **54**, 395302 (2021).
- [17] H. Friedman, D. A. Kessler, and E. Barkai, Quantum renewal equation for the first detection time of a quantum walk, *J. Phys. A: Math. Theor.* **50**, 04LT01 (2017).
- [18] H. Friedman, D. A. Kessler, and E. Barkai, Quantum walks: The first detected passage time problem, *Phys. Rev. E* **95**, 032141 (2017).
- [19] Q. Liu, R. Yin, K. Ziegler, and E. Barkai, Quantum walks: The mean first detected transition time, *Phys. Rev. Res.* **2**, 033113 (2020).
- [20] P. W. Shor, Scheme for reducing decoherence in quantum computer memory, *Phys. Rev. A* **52**, R2493 (1995).
- [21] S. Lloyd, Universal quantum simulators, *Science* **273**, 1073 (1996).

- [22] R. Hicks, B. Kobrin, C. W. Bauer, and B. Nachman, Active readout-error mitigation, *Phys. Rev. A* **105**, 012419 (2022).
- [23] J. M. Günther, F. Tacchino, J. R. Wootton, I. Tavernelli, and P. K. Barkoutsos, Improving readout in quantum simulations with repetition codes, *Quantum Sci. Technol.* **7**, 015009 (2022).
- [24] Qiskit, <https://github.com/Qiskit> (IBM, Armonk, 2021).
- [25] A. M. Childs, E. Deotto, E. Farhi, J. Goldstone, S. Gutmann, and A. J. Landahl, Quantum search by measurement, *Phys. Rev. A* **66**, 032314 (2002).
- [26] D. Herman, R. Shaydulin, Y. Sun, S. Chakrabarti, S. Hu, P. Minssen, A. Rattew, R. Yalovetzky, and M. Pistoia, Portfolio optimization via quantum Zeno dynamics on a quantum processor, [arXiv:2209.15024](https://arxiv.org/abs/2209.15024).